Polystyrene Hydrogenolysis to High-Quality Lubricants using Ni/SiO_2

Brandon C. Vance[1,2], Sean Najmi[1], Dionisios G. Vlachos[1,2]*

AUTHOR ADDRESS

[1]Center for Plastics Innovation, University of Delaware, 221 Academy St., Newark, DE 19716, USA

[2]Department of Chemical and Biomolecular Engineering, University of Delaware, 150 Academy St., Newark, DE 19716, USA

*Corresponding author: vlachos@udel.edu

KEYWORDS

Plastics Waste; Hydrogenolysis; Nickel; Earth-abundant Metals; Lubricants

ABSTRACT

Pyrolytic and light-activated oxidation processes are leading technologies for utilizing polystyrene (PS) wastes. These approaches exhibit poor selectivities, use complex reactors, and require solvents. Hydrogenolysis is effective for deconstructing polyolefins, but its application to PS feedstocks has been limited. Herein, we demonstrate Ni/SiO_2 catalysts to facilitate PS (M_w ~97 kDa) hydrogenolysis to produce lubricant base oils possessing Group IV properties, achieving maximum yields of 70% within 6 h at 300 °C and 70 bar H_2. Gas, liquid, and oil product yields are stable across reaction conditions, whereas hydrogenation of the PS aromaticity and reduction of the molecular weight benefit from higher temperatures and H_2 pressures. Time-dependent experiments underscore the importance of elevated H_2 pressure, revealing PS hydrogenolysis occurs sequentially, with aromatic ring hydrogenation preceding degradation of the C-C backbone. Kinetic measurements with 1,2-diphenylethane as a probe molecule demonstrate ring hydrogenation is three orders of magnitude faster than internal C-C bond cleavage over Ni/SiO_2. Ni/SiO_2 proves effective in the hydrogenolysis of heavier PS polymers and rigid commercial PS products. Conversely, flexibility and foam PS feeds result in Ni/SiO_2 deactivation, attributed to performance additives. Unlike polyolefins, the process produces very little methane and other light hydrocarbons. These findings expand the applicability of hydrogenolysis to PS feedstocks, offering a versatile solution and broadening the range of high-value products from PS to include lubricant base oils.

1. Introduction

The massive scale of plastic utilization and unsustainable disposal of plastic waste have resulted in extensive strain on global ecosystems[1–4] and significant consumption of the global carbon budget[5–8]. A paradigm shift in the plastics waste industry is urgently needed to drive the transition from today's linear (take, make, and waste) economy[9] to a future circular one. Mechanical recycling is a mature, cost-effective technology[8,10,11] for polyethylene terephthalate and high-density polyethylene. Other thermoplastics are primarily diverted to landfills or incinerators[5,6].

Chemical recycling is promising for utilizing these wasted thermoplastics. Polyethylene and polypropylene feedstocks have curated the most attention, with demonstrations of pyrolysis[12–14] and hydroconversion[15–25] producing light olefins, alkylaromatics, fuel-range hydrocarbons, naphtha, lubricant-base oils, and more. Polystyrene (PS) feedstocks have attracted considerably less attention. PS pyrolysis[26–32] in an N_2 atmosphere has been demonstrated for styrene monomer recovery at high reaction temperatures (400-600 °C). Polycyclic tar oils are a problematic byproduct of pyrolysis due to the poor selectivity of the radical-mediated chemistry[33,34]. Reactor configurations that incorporate continuous separation of the gas phase (i.e., reactive distillation, fluidized bed, semi-continuous batch, etc.) can boost styrene yields as high as 70-80%. Kumar et al. demonstrated that the addition of copper and sodium chloride catalysts can further enhance styrene yields to 84%. Light-activated oxidation of PS[35–41] to produce oxygenated aromatics (benzoic acid, benzaldehyde, acetophenone, etc.) at ambient conditions has also been demonstrated, but these chemistries must be conducted with solvents and complex catalysts while exhibiting limited selectivity control and low carbon efficiencies. Biosynthetic oxidative routes for PS have also been demonstrated with fungal strains generating pharmacologically relevant

molecules[42], while engineered bacterium produces oxygenated monomers[43]. The hydrogenation of PS to polyvinyl-cyclohexane (PVCH) using nickel, cobalt, and platinum-based catalysts was reported during the mid-20th century[44–47]. The studies utilized dissolved PS with moderate reaction temperatures (200-300 °C) and high H_2 pressures (140-265 bar) to achieve complete hydrogenation, often accompanied by polymer molecular weight degradation. Recently, solvent-free PS hydrogenolysis using Ni/SiO_2 was introduced as a proof-of-concept for selectively generating heavy liquid oils at similar temperatures and significantly lower H_2 pressure (30 bar cold)[15]. Hydrogenolysis did not produce byproduct tar oils seen in pyrolysis, highlighting the benefit of hydrogenative catalysts in quenching this undesired pathway. The development of this process is an appealing strategy to create high-value products while expanding the product slate from PS deconstruction.

Herein, we demonstrate the optimized hydrogenolysis of PS with Ni/SiO_2 catalysts for producing high-quality lubricant-base oils. Ni/SiO_2 shows direct reusability for 4 cycles with no deactivation. The chemical structure of these oils and flow properties are analyzed. The reaction network is proposed based on time-dependent experiments with PS and 1,2-diphenylethane as a model molecule. This process is extended to polystyrenes of various molecular weights and commercial PS products. This work expands the scope of polyolefin hydrogenolysis to PS feedstocks and diversifies the existing product slate of PS conversion technologies to include lubricant base oils.

2. Results and Discussion

2.1. Effect of Reaction Conditions on PS Deconstruction

The reaction temperature and H_2 pressure (P_H) were shown to strongly influence the nickel's catalytic activity for the hydrogenation/hydrogenolysis of PS dissolved in decalin[46] and low-density polyethylene hydrogenolysis[15]. Solvent-free hydrogenolysis of PS97 (M_w ~97 kDa, Sigma) was operated in semi-batch H_2 to maintain a constant $P_H \pm 2$ bar and washed with methanol to collect light hydrocarbons (i.e., alkanes, aromatics, and oligomers), and then methylene chloride to collect heavy oils for product collection (see Methods). Fig. 1a-b, Fig. S1, and Table S1 display the product yields from the temperature and P_H screening, respectively. Catalyst characterization has been reported previously[15]. Excitingly, methane and other gaseous hydrocarbon production is negligible for PS hydrogenolysis, whereas methane is a major byproduct in PE and PP hydrogenolysis[15,16,18–20]. Minor yields of liquid alkanes, aromatics, and oligomers (<10% each) were detected in the methanol wash. The alkane and aromatic hydrocarbons all contained alkyl chains with 1-4 carbons, while oligomers consisted of fully and partially hydrogenated derivatives of the PS dimer and trimer, per GCMS (Fig. 1c). Heavy oils, which are methanol-insoluble and comprised of unreacted and degraded PS, are the dominant products, regardless of reaction conditions. Mass balances span 75-98%, with harsher conditions consistently resulting in less oil and lower mass balances. The unquantified mass is associated with large oligomers (tetramers, pentamers, etc.) that are methanol-soluble but are too heavy to elude during GC analysis (see Hydrogenolysis Time-Dependence). Unfortunately, little information on the impact of temperature and P_H on the PS97 hydrogenolysis is attainable by purely analyzing the product yields.

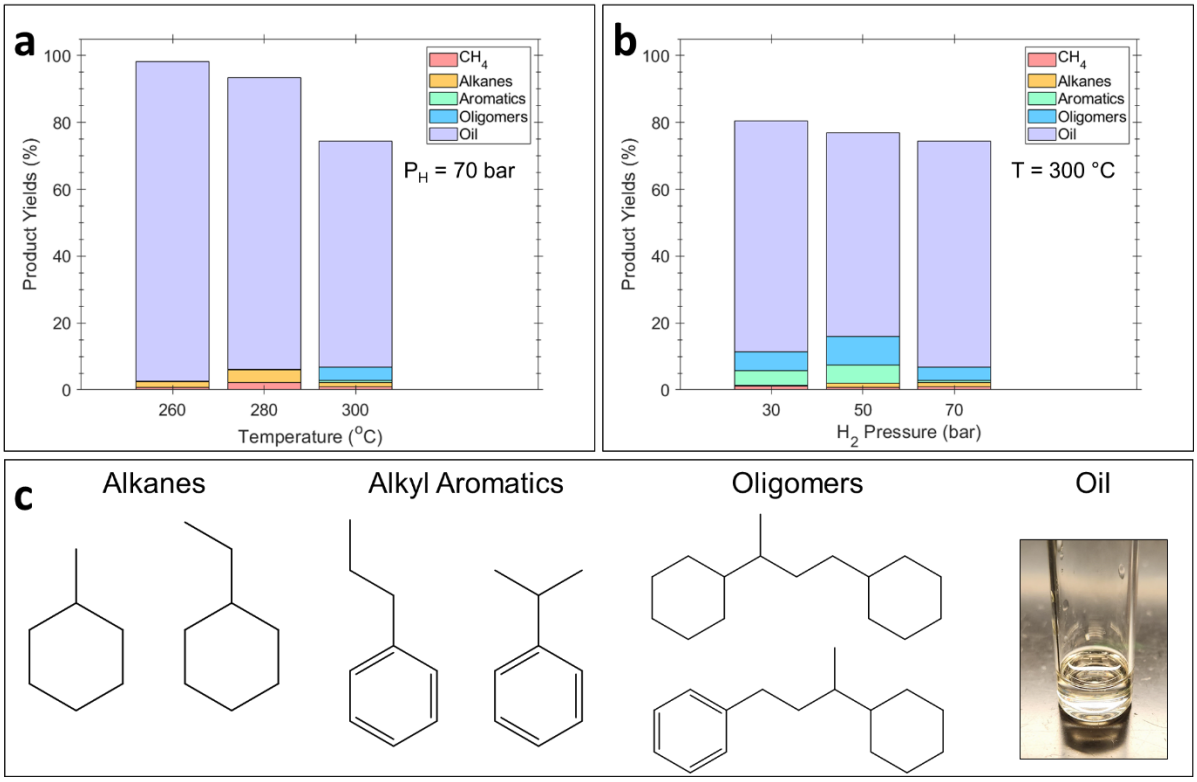

Figure 1: ***Reaction condition screening for PS97 hydrogenolysis. a,*** *and* ***b****, Product yields as a function of reaction temperature and H_2 pressure, respectively.* ***c****, Common alkanes, alkyl aromatics, and oligomers in product fractions and a picture of product oil. Reaction conditions: 2 g PS97, 100 mg Ni/SiO_2, 2 h, semi-batch H_2. Pressures are at the reaction temperature.*

Gel-permeation chromatography (GPC) can determine changes in the product oils' molecular weight distributions (MWD). GPC of the neat PS97 shows a trimodal distribution with molecular weights centered at ~4.5 kDa, ~78 kDa, and ~7300 kDa (Fig. 2, Fig. S2-4, and Table S2-3) with an overall average molecular weight (M_w) of ~97 kDa. Upon PS97 hydrogenolysis at 260 °C and 30 bar H_2, the oil's MWD is effectively the same as the neat PS97 MWD with a slight downward shift in the heaviest mode's center from ~7500 kDa to ~4600 kDa (Fig. 2a, Table S2-3). Increasing P_H to 70 bar while maintaining the reaction temperature shows identical changes in the oil's MWD with a comparable downward shift in the heaviest mode (Fig. 2b, Table S2-3). Alternatively, increasing the reaction temperature to 300 °C results in a growth of a ~2.6 kDa mode yield and a

concurrent downward shift in the heaviest mode's position from ~7500 kDa to ~1800 kDa for both pressures (Fig. 2c-d, Table S2-3).

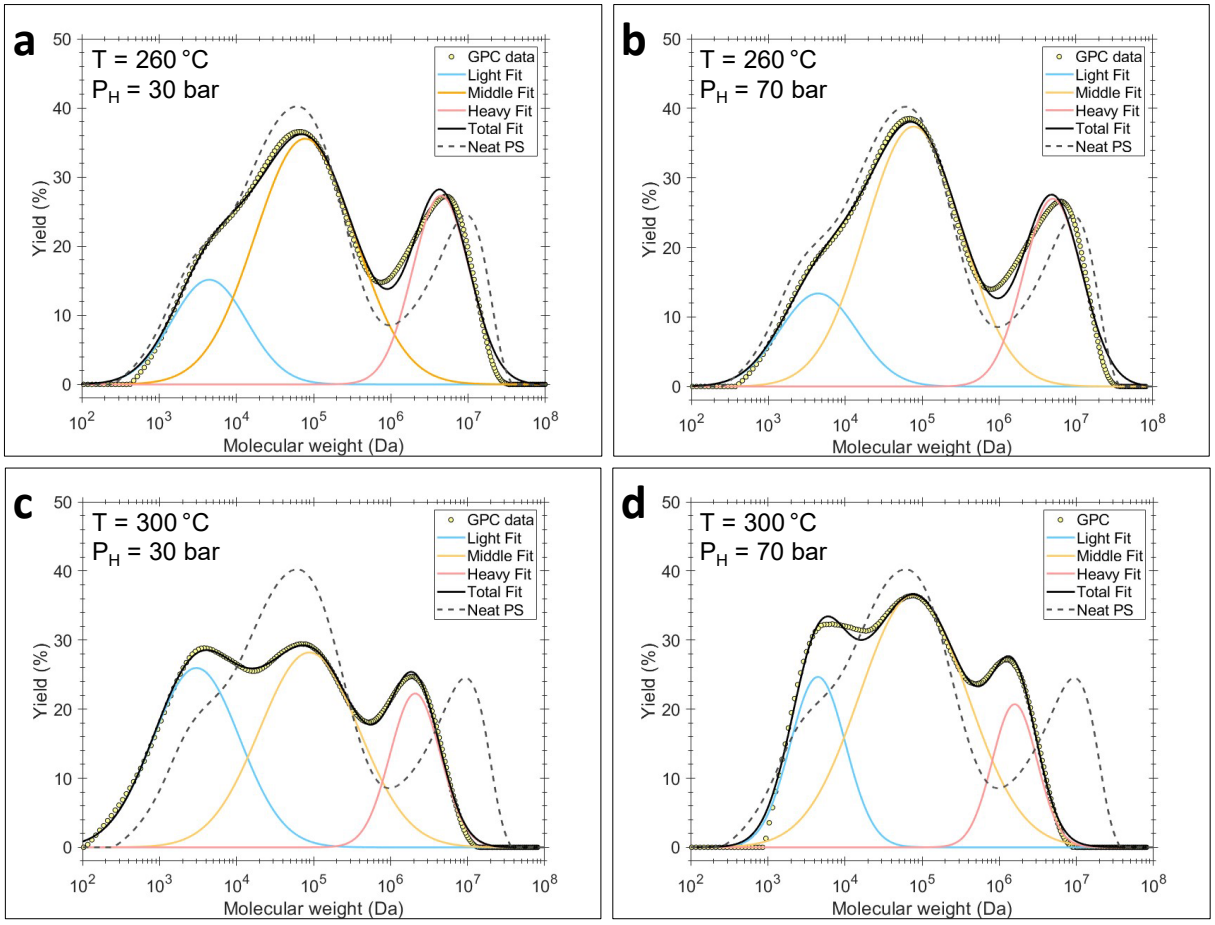

Figure 2: ***Yield distributions from GPC of methanol-insoluble oils with deconvolutions from the reaction condition screening for PS97 hydrogenolysis.*** *Reaction conditions: 2 g PS97, 100 mg Ni/SiO_2, 2 h, semi-batch H_2. Pressures are at the reaction temperature.*

Liquid ^{1}H nuclear magnetic resonance (NMR) provide insights into the changes to the PS97 chemical structure upon hydrogenolysis. Product oils from hydrogenolysis at 300 °C show significant differences in the alkyl (0 – 2.5 ppm) and aromatic regions (6 – 8 ppm) of the ^{1}H spectra when increasing P_H from 30 bar to 70 bar (Fig. 3a-b, Fig. S5-7. Fig. 3a shows the ^{1}H protons bound in methine groups from 1.58 - 1.8 ppm (blue), long-chain primary carbons from 0.82 – 0.92 ppm

(orange), and short-chain primary carbons at 0.66 – 0.92 ppm (green). Raising P_H shows a monotonic growth for these alkyl protons. Methine and primary long-chain groups have the largest relative growth, indicating the hydrogenolysis and hydrogenation of the aromatic ring increases with higher pressures of hydrogen. Additionally, the non-uniformity in the splitting indicates there may be several different components present in the oil product.

Similarly, a broad band spanning 1.0-1.3 ppm also appears in the NMR spectra, becoming the most intense for oils reacted at 70 bar H_2 (Fig. 3a-b). The center of this band spanning 1.1-1.2 ppm is assigned to methine protons adjacent to cyclohexyl-sidechains (purple in Fig. 3b), based on the reference spectra of PVCH (Fig. S8). Examination of the proton adjacent to aromatic region (2.5-2.8 ppm) corroborates the effect of hydrogen pressure on the concentration of aromatic rings within the polymer (red in Fig. 3b). Increasing P_H results in a drop in the abundance of aromatic protons with a concomitant generation of methine protons adjacent to cyclohexyl sidechains. These observations provide insight into the PS hydroconversion mechanism. To simplify the analysis while capturing the changes to the PS chemical structure, we define the alkyl-to-aromatic ratio (AAR); the ratio of all aliphatic protons to all aromatic protons (see Methods). The AAR of neat PS97 was 0.6, matching the theoretical value of a polystyrene polymer (Fig. 3c). The AAR of the oils from PS97 hydrogenolysis at 300 °C shows a strong increase with P_H, as expected from Fig. 3a and b, with a maximum AAR = 2.58 achieved at 70 bar H_2. Furthermore, the AAR increases with P_H for the 280 °C oils, but the magnitude is less significant, with a maximum AAR = 1.72. Interestingly, P_H does not impact the AAR for the 260 °C oils, with AAR values fluctuating around ~1.0, indicating there are likely kinetic barriers given that hydrogenation is highly favored by thermodynamics (Table S4).

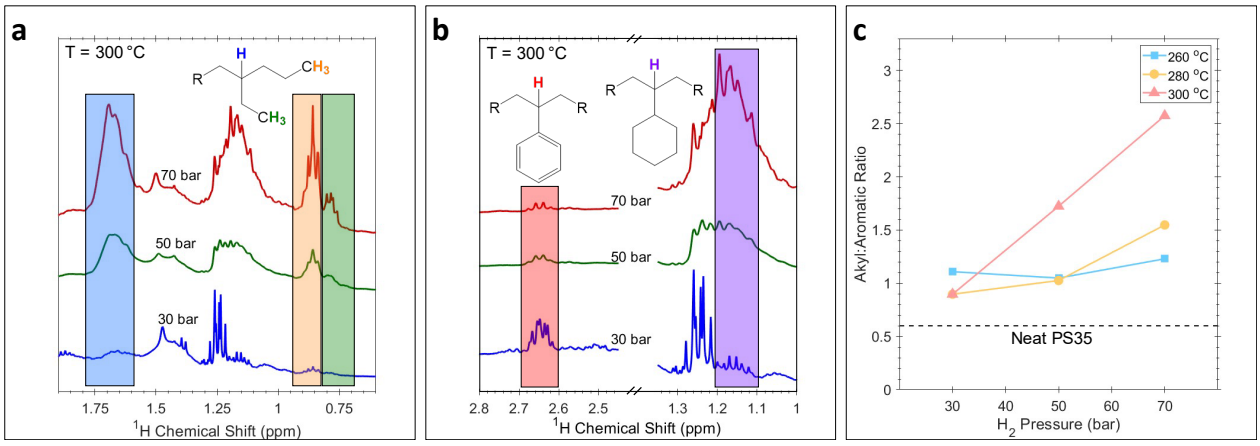

Figure 3: ***¹H NMR of methanol-insoluble oils from the reaction condition screening for PS97 hydrogenolysis. a, and b,*** *Aliphatic ¹H region. b, Comparison of secondary ¹H regions for protons in the polymer backbone adjacent to aromatic and alicyclic chemical environments. c, AAR for each of the product oils. Reaction conditions: 260-300 °C, 30-70 bar H_2, 2 g PS97, 100 mg Ni/SiO_2, 2 h, semi-batch H_2. Pressures are at the reaction temperature.*

Overall, this parametric study demonstrates that the product (oils, liquids, and CH_4) yields are unaffected by temperature and P_H, but the oils are distinct. Both GPC and liquid ^{1}H NMR elucidate that these parameters strongly influence the molecular weight distribution and chemical structure of the hydrogenolysis oils, respectively. Higher reaction temperatures and P_H facilitate deeper hydrogenation and hydrogenolysis of the PS97; thus, 300 °C and 70 bar H_2 are primarily used next.

2.2. Thermal Degradation without Ni/SiO₂

Fig. 4a and Table S5 show the product yields for reactions at 300 °C and 70 bar H_2 with and without Ni/SiO_2 to probe the influence of thermal degradation. Reactions without catalyst generate 64% oil yields and 39% yields of methanol-soluble products, comprised mostly of alkylaromatics and oligomers. The oils from hydrogenolysis without catalyst from thermal degradation are black tar-like oils compared to the clear oils attained over Ni/SiO_2. ^{1}H NMR of the noncatalytic oils reveal a low AAR of 0.5, below the AAR of PS, with large concentrations of aromatic groups still present (Fig. 4b and Fig. S9). Additionally, the PS conversion based on ^{1}H NMR analysis (see

Methods) is twofold higher for the noncatalytic test than the Ni/SiO_2 (Fig. 4b). GPC of the noncatalytic oils unveils a broad molecular weight distribution spanning < 0.1 kDa to ~2000 kDa with a maximum at ~1100 kDa (Fig. 4c), exposing massive molecular weight degradation due to thermal reactions. Conversely, the GPC of the catalytic hydrogenolysis oils show a reduction of the molecular weight of the heaviest molecular weight mode ~7500 kDa to ~1800 kDa. These results indicate Ni/SiO_2 suppresses thermal degradation reactions of PS97 and shifts the reaction chemistry to purely hydrogenation/hydrogenolysis over the Ni surface. Thermal degradation is much faster than hydrogenolysis for reducing the polymer's molecular weight, but the trade-off is the improved selectivity over Ni/SiO_2.

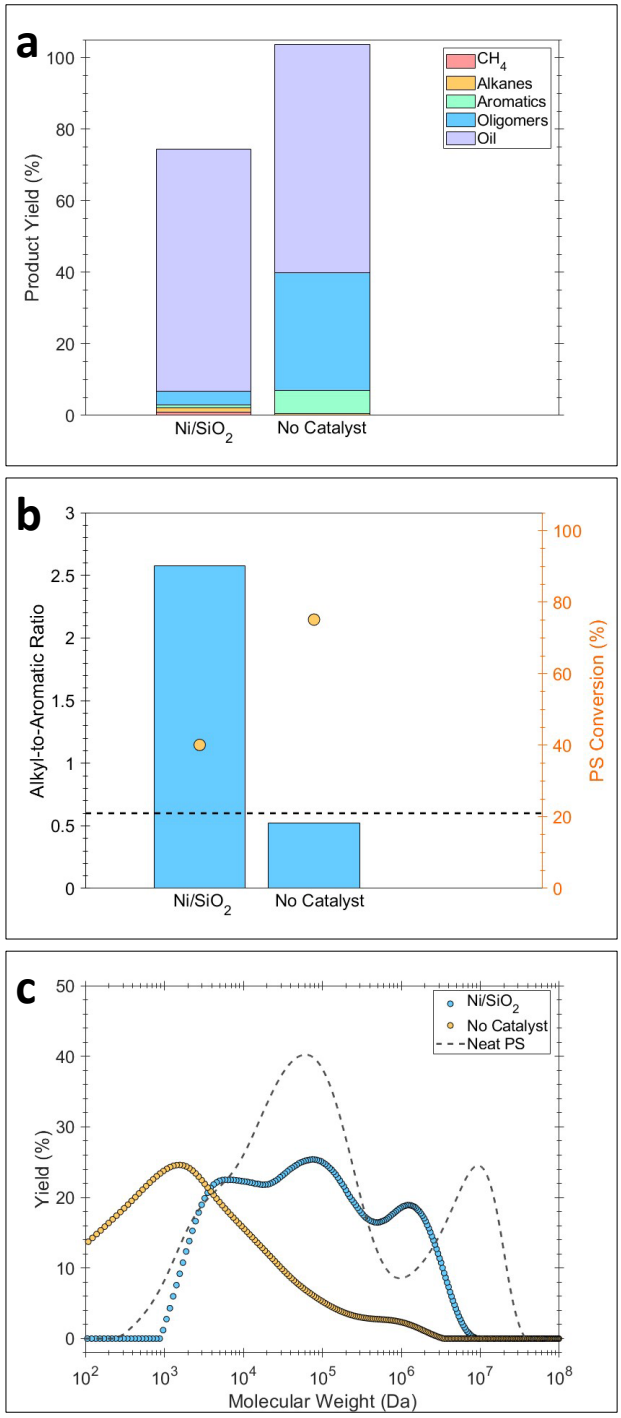

Figure 4: ***PS97 hydrogenolysis with and without Ni/SiO₂. a,*** *Product yields.* ***b,*** *Alkyl-to-aromatic ratio.* ***c,*** *Yield distributions from GPC of methanol-insoluble oils****.*** *Reaction conditions: 300 °C, 70 bar H_2 at reaction temperature, 2 g PS97, 100 mg Ni/SiO_2 or no catalyst, 2 h, semi-batch H_2.*

2.3. Hydrogenolysis Time-Dependence

Time-dependent hydrogenolysis experiments were conducted to explore the P_H effect at 300 °C and gain insights into the reaction network. PS97 hydrogenolysis spanning 0.5-9 h at 30 and 70 bar H_2 are shown in Fig. 5 and Table S6. Oil and liquid (i.e., methanol-soluble) product yields are effectively identical between the two P_H and stable across the reaction span (Fig. 5a). However, liquid yields at 70 bar display a substantial increase at 9 h due to the generation of oligomers (Fig. S10). This test has full closure of the mass balance, while the average balance for the other time-dependent experiments is ~82%. The quantified oligomer fraction only accounts for the PS dimer, trimer, and their derivatives. The spike in oligomer yields for the 9 h reaction at 70 bar suggests they form from larger oligomer fragments (tetramers, pentamers, etc.) that are methanol-soluble but too heavy to be eluded during the GC analysis. Akin to the reaction condition screening, product yields provide limited insights requiring oil characterization with NMR and GPC.

Liquid ^{1}H NMR (Fig. 5b) and GPC (Fig. 5c) reveal a substantial difference in the time-dependent behavior of the AAR and average M_w, respectively, at 30 and 70 bar H_2. The AAR of the 30 bar oil has a minor increase from the neat PS value of 0.6 to ~1.1 in 0.5-4 h, with longer reaction times showing little change (Fig. 5b and Fig. S11). The MWD of the oil closely resembles that of the neat PS97 with a downward shift in the heaviest mode's center from ~7300 kDa to ~1600 kDa over the entire reaction span (Fig. S12). Deconvolution of the MWD indicates minor redistribution of the weight fractions for the two lightest modes (~4.5 kDa and ~77 kDa), while the heaviest mode's weight fraction is stable (Fig. 6a). Overall, the MWD changes culminate to a moderate reduction in the average M_w from ~97 kDa to ~57 kDa for the 30 bar oil, that is achieved within 0.5 h before plateauing at longer times (Fig. 5c). The low, stationary AAR coupled with the

stagnant average M_w expose that 30 bar H_2 is insufficient for Ni/SiO_2 to facilitate hydrogenation and hydrogenolysis.

Conversely, the 70 bar oils display a linear growth in the AAR to 4.5 in 1-4 h, and 12.2 at 6 h (Fig. 5b and Fig. S13). The MWD also demonstrates significant changes in the 1-6 h time span as the weight fraction of the heaviest mode (~2300 kDa) is gradually reduced from ~20 wt% to 0 wt%, with a concurrent growth of the lightest mode (~4.5 kDa) from ~25 wt% to ~60 wt% (Fig. 6b and Fig. S14). The elimination of the heaviest mode results in a substantial reduction in the average M_w to ~13 kDa in 6 h (Fig. 5c). Extending the reaction time to 9 h shows minimal improvement in the AAR (Fig. 5b), MWD weight fractions (Fig. 6b), and average M_w (Fig. 5c). The resulting oils at 6 h and 9 h are completely bimodal and have effectively identical MWD (Fig. 6c and Fig. S14).

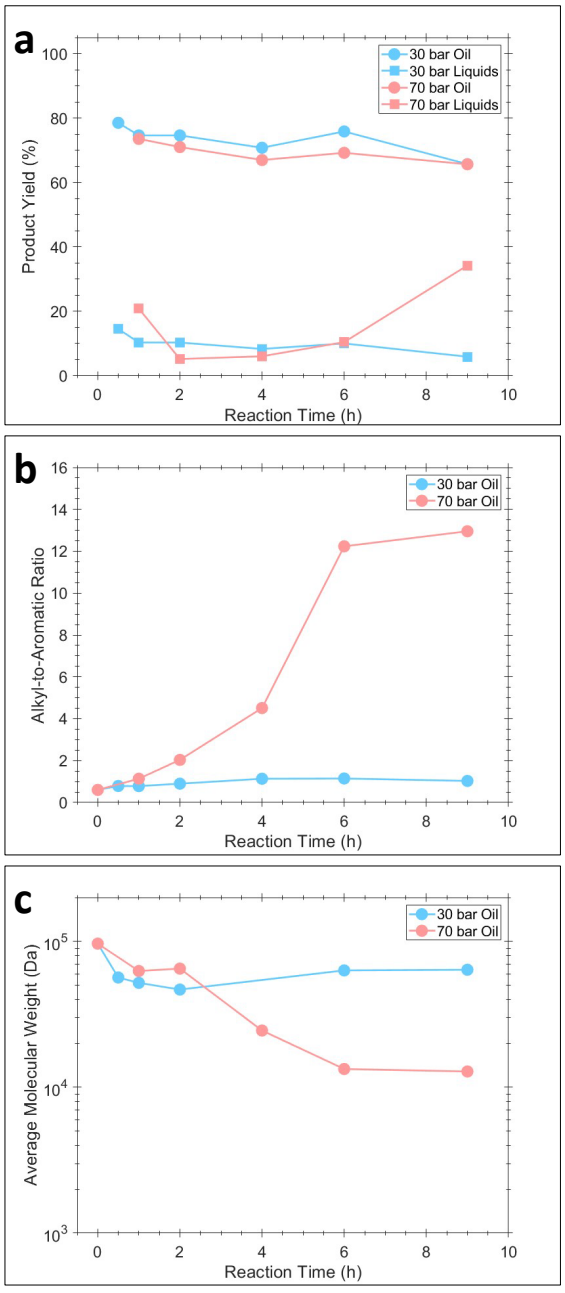

Figure 5: ***Time-dependent PS97 hydrogenolysis at 30 and 70 bar H_2. a,*** *Liquid and oil product yields as a function of reaction time.* ***b,*** *AAR for the product oils calculated from ^{1}H NMR.* ***c,*** *Average molecular weights of the product oils calculated from the GPC. Reaction conditions: 300 °C, 2 g PS97, 100 mg Ni/SiO_2, semi-batch H_2. Pressures are at the reaction temperature.*

These findings demonstrate the importance of high P_H for Ni/SiO_2 to facilitate PS97 hydrogenolysis. Hydrogenolysis of the PS backbone only occurs after significant hydrogenation of the aromatic rings, suggesting a sequential reaction network. Furthermore, the reduction in the average M_w is dominated by the deconstruction of the heaviest polymer chains (M_w > ~100 kDa),

while lighter molecular weight chains show limited deconstruction. The lower reactivity of these lighter chain fragments may stem from weaker surface adsorption that result in short surface residence times. Reaction rate analysis (see Probe Reactions with 1,2-Diphenylethane (DPE)) reveals C-C bond scission rates are 1000x slower than aromatic ring hydrogenation. These slow reaction rates demand long surface residence times, which are unlikely for lighter molecular weight species. The presence of strong surface adsorption has been revealed for polyolefin systems[15,23,48,49], with major mechanistic insights, such as the adhesive isomerization cycle[23] and the divergent hydrogenolysis mechanism[15] in PE hydrocracking and hydrogenolysis, respectively.

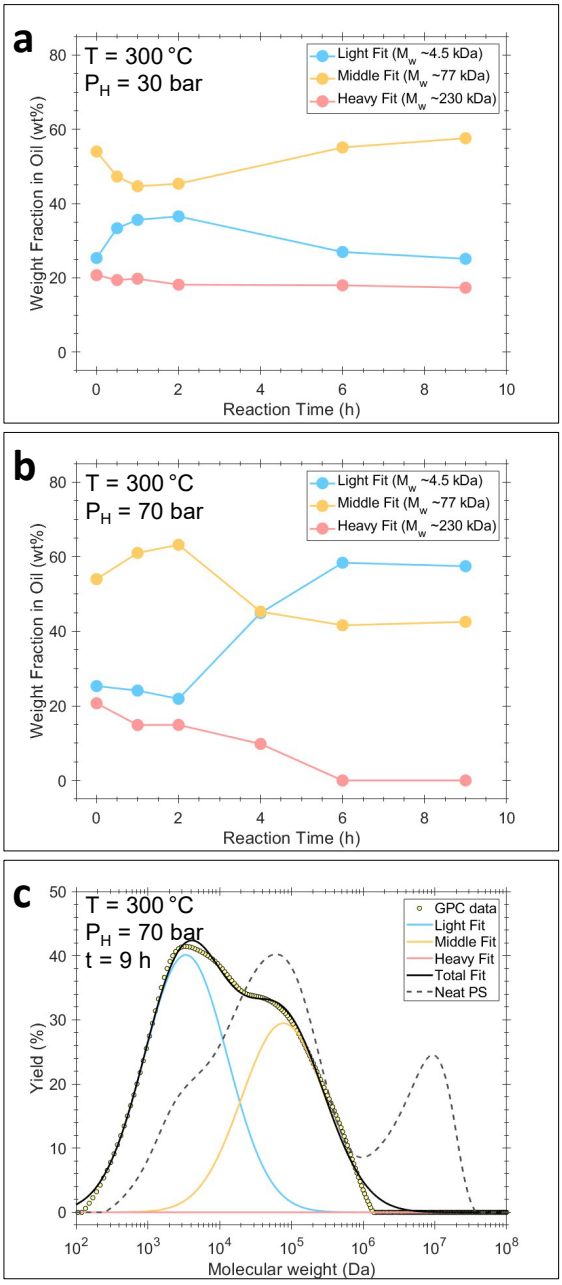

Figure 6: ***GPC analysis for the oils from the time-dependent PS97 hydrogenolysis at 30 and 70 bar H_2. a,*** *and* ***b,*** *Weight fractions for the three Gaussian modes fit to the GPC yield curves at 30 and 70 bar H_2, respectively.* ***c,*** *Yield distributions of the product oils after 9 h of reaction time at 30 and 70 bar H_2, respectively. Reaction conditions: 300 °C, 2 g PS97, 100 mg Ni/SiO_2, semi-batch H_2. Pressures are at the reaction temperature.*

The hydrogenolysis oils from the long reaction times (6-9 h) at 300 °C and 70 bar H_2 were clear and flowed easily, suggesting these oils are good candidates for lubricant base-oil applications. Table 1 shows the measured properties of the PS97 oils from the 6 h reaction

compared to a commercial synthetic lubricant base oil and oils obtained from polypropylene (PP) hydrogenolysis[22]. High-quality lubricants typically demand low pour points, high oxidation onset temperature, and high viscosity indices (VI) as these reflect the oil's ability to flow at low temperatures, its thermal stability, and the viscosity dependence on temperature, respectively. The VI is a primary parameter for classifying lubricant qualities, with lower-grade Group I-III oils having VI < 120 and high-grade Group IV oils having VI > 120 [50,51]. The PS97 oil has a high VI of 130 ± 2, qualifying as a Group IV oil. This VI is lower than but comparable to the reported PP oils and the Chevron PAO6. The pour point and oxidation onset for the PS97 oil outperform the PP oils but are inferior to the commercial PAO6. The kinematic viscosity (KV) of PS97 oil is approximately double that of the light PP oil and Chevron PAO6, meaning these oils are not suitable for identical applications. High KV lubricants are commonly used in heavy machinery applications. However, flow additives could be used to tailor the KV and VI of the PS97 oils to be more comparable to PAO6. Overall, these properties identify lubricant base oils as an attractive application for the PS97 oils.

Table 1: Analysis of oil properties from PS97 hydrogenolysis and comparison with commercial lubricant base oils and previously reported oils from plastics waste hydrogenolysis. [A] ASTM D5949. [B] ASTM E2009. [C] KV40 and KV100 are kinematic viscosities measured at 40 and 100 °C, respectively. [D] Calculated from KV40 and KV100. [E] Commercial synthetic base oil from Chevron; oil properties are from the manufacturer specifications sheet. [F] Oil properties reported from PP hydrogenolysis with Ru/TiO_2 in ref[22]. Reaction conditions: 300 °C, 70 bar H_2, 2 g PS97, 100 mg Ni/SiO_2, 6 h, semi-batch H_2.

Sample	**Pour Point (°C)[A]**	**Oxidation Onset (°C)[B]**	**KV40 (cSt)[C]**	**KV100 (cSt)[C]**	**Viscosity Index[D]**
PS97 Oil (6 h)	-30	184	79.8 ± 0.9	11.2 ± 0.2	130 ± 2
Chevron PAO6[E]	-62	246	30.8	5.9	139
Light PP Oil[F]	-15	179	30.3 ± 0.2	6.2 ± 0.1	146 ± 7
Heavy PP Oil[F]	-18	175	113.5 ± 0.8	42.2 ± 0.3	149 ± 7

2.4. Probe Reactions with 1,2-Diphenylethane (DPE)

DPE was used as a model molecule to probe the PS97 hydrogenolysis reaction mechanism. Three-phase continuous flow experiments reveal that DPE consumption rates have Arrhenius behavior with a strong P_H dependence, like PS97 hydrogenolysis (Fig. S15-16). Unfortunately, full DPE conversion in continuous flow was difficult to attain due to the high H_2 stoichiometry (6 mol H_2 to 1 mol DPE) that resulted in rapid H_2 depletion. Time-dependent experiments in the semi-batch H_2 system were first run instead to map the reaction progression (Fig. 7a) at 300 °C and 50 bar H_2. Initial semi-batch H_2 experiments revealed that DPE was substantially more reactive than PS97, requiring the Ni/SiO_2 loading to be limited to 5-20 mg and increasing the substrate mass to 3 g to access the kinetic envelope. Time-dependent experiments reveal that the aromatic rings of DPE are sequentially hydrogenated to produce 1,2-cyclohexylbenzylethane (CHBE), and then 1,2-dicyclohexylethane (DCHE) (Fig. 7a-b, Fig. S17). Surprisingly, only minor quantities of methylcyclohexane (MCH) were detected, and toluene (TOL) or products from ring-opening reactions were not detected. Longer DPE residence times (τ) increase the MCH production. Comparison of initial rates demonstrates DPE and CHBE hydrogenation rates are approximately identical ($r{\sim}10\ mmol_{arene} \cdot min^{-1}$), whereas the MCH production (i.e., DCHE hydrogenolysis, $r{\sim}0.01\ mmol_{C-C} \cdot min^{-1}$) is 1000x times slower. These rate differences could justify the MWD stability of the PS97 oils after long times, but conflict with the relatively fast degradation of the heaviest PS modes after hydrogenation (Fig. 5 and Fig. 6). Elias et al.[46] reported on the hydrogenation of dissolved PS to PVCH with a final M_w ~62 kDa using Raney-Ni catalyst and proposed that the PS molecular weight degradation was due to thermal and mechanical effects rather than direct hydrogenolysis. The DPE rate analysis and PS97 hydrogenolysis reactions support these findings; yet it is unclear why chains below M_w ~100 kDa are less prone to deconstruction.

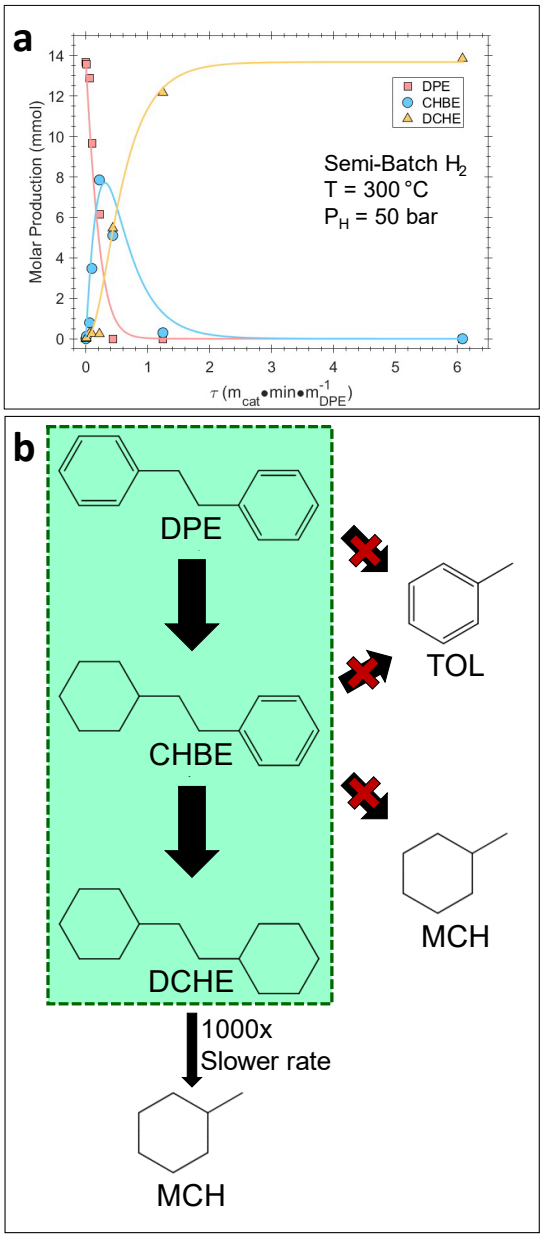

Figure 7: ***Hydrogenolysis kinetics of the probe molecule 1,2-diphenylethane (DPE)****.* ***a,*** *and* ***b,*** *Kinetic evolution of major reaction products in a semi-batch H_2 reactor and respective DPE hydrogenolysis reaction pathway. Reaction conditions: 300 °C, 50 bar H_2 at reaction temperature, 3 g DPE, 5-20 mg Ni/SiO_2, 0.5-6 h, semi-batch H_2.*

Interestingly, Ni/SiO_2 has previously been shown to facilitate internal C-C bond cleavage of n-hexacosane (nC26) with hydrogenolysis rates of ~0.1 $mmol_{C-C} \cdot \text{min}^{-1}$.[15] There is an order of magnitude difference in the internal C-C bond hydrogenolysis rates between nC26 and DCHE (i.e., the rate of DCHE consumption) suggesting the carbon structure of DCHE is unable to form the

same surface ensembles of nC26, forcing DCHE hydrogenolysis through a higher energy transition state[52]. Moreover, nickel's sensitivity to the hydrocarbon structure and limited ring-opening capacity is well-established[53–56]. This surface ensemble effect also rationalizes why ring-opening reactions are not observed in DPE hydrogenolysis and the cyclohexyl side chains in the PS97 oils remain intact.

2.5. Ni/SiO_2 Catalyst Reuse

Catalyst reuse is a valuable metric in determining the industrial viability of a catalyst[57]. Spent Ni/SiO_2 was collected after the 6 h reactions at 300 °C and 70 bar H_2 by filtration and dried in air at 25 °C before testing for direct reusability for PS97 hydrogenolysis. Fig. 8a shows that the oil and liquid product yields are stable over four reuse cycles. Conversely, the oils' AAR from liquid ^{1}H NMR increases from 12.2 to 18.9 over the first two reuses and stabilizes at further reuses. The improved AAR over each reuse demonstrates Ni/SiO_2 does not deactivate; on the contrary, its hydrogenation performance improves with each cycle. Thermogravimetric analysis of the Reuse-4 catalysts indicates minimal coking (<1wt%) on the catalyst surface (Fig. S18). Comparing the X-ray diffraction (XRD) of fresh and Reuse-4 Ni/SiO_2 reveals partial restructuring of the Ni nanoparticle morphology from the Ni(200) facet at 44.6° to the Ni(111) facet at 52.0° (Fig. 8b). The Ni(111) facet is the primary active phase in benzene hydrogenation as it readily activates the C-H bond due to the close symmetry in the Ni lattice spacing and C-C aromatic bond length[58,59]. Subsequently, the increased Ni(111) fraction rationalizes the improved activity upon reuse.

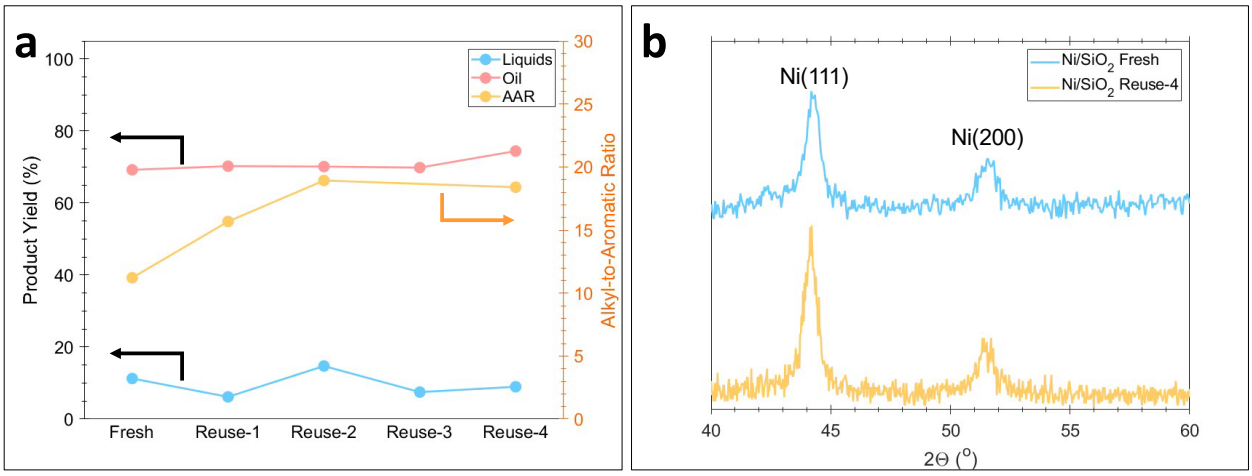

Figure 8: ***Direct Ni/SiO2 reuse for PS97 hydrogenolysis. a,*** *Liquid and oil product yields with the oil AAR calculated from ^{1}H NMR.* ***b,*** *XRD catalyst of the fresh and reuse-4 Ni/SiO_2 catalyst. Reaction conditions: 300 °C, 70 bar H_2 at reaction temperature, 2 g PS97, 100 mg catalyst, 6 h, semi-batch H_2.*

2.6. Feedstock Variation

Other virgin and commercial PS feedstocks were used to probe the versatility of Ni/SiO_2 for PS hydrogenolysis at 300 °C, 70 bar H_2, and 9 h. Hydrogenolysis of virgin PS5300 and PS6000 feedstocks produce 67% and 69% oil yields, respectively, comparable to 66% of PS97 (Fig. 9a). Interestingly, liquid product yields are >25% lower for PS5300 and PS6000 due to a reduction in oligomers likely due to the heavier M_w of these feedstocks that produce heavy oligomers (tetramers, pentamers, etc.) not detectable by GC. The high AAR of the PS5300 and PS6000 oils indicates considerable hydrogenation (Fig. 9b and Fig. S19). However, there is not a clear trend between AAR and molecular weight as the PS5300 oil's AAR is comparable to that of the PS35 oils while the PS6000 oil's AAR is ~50% lower than the latter two, demonstrating a lower activity for PS6000. The differences in the virgin PS reactivities could stem from molecular weight, architecture, or viscosity[21,60], and slip agents or other performance additives may be present and inhibit the deconstruction[17,25].

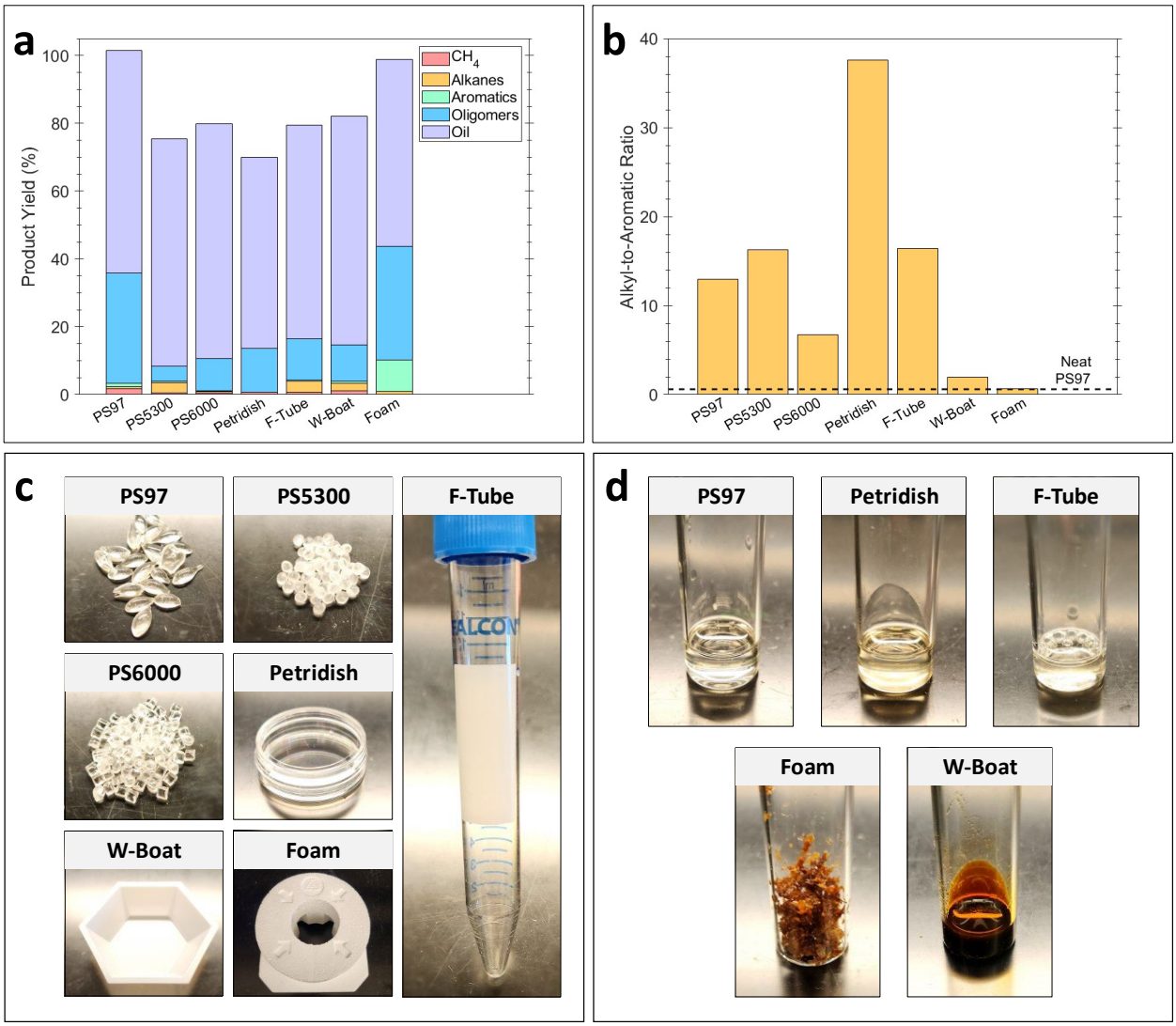

Figure 9: ***Hydrogenolysis feedstock variation including virgin and commercial polymer products. a,*** *Product yields.* ***b,*** *AAR for the product oils calculated from ^{1}H NMR.* ***c,*** *and* ***d,*** *Pictures of raw PS feedstocks and resulting products from hydrogenolysis reactions, respectively. Reaction conditions: 300 °C, 70 bar H_2 at reaction temperature, 2 g substrate, 100 mg Ni/SiO_2, 9 h, semi-batch H_2.*

Hydrogenolysis of commercial PS products (Fig. 9c) shows wide variability in reactivity. Rigid PS products (i.e., Petridish and F-Tube) produce clear, inviscid oils with high AARs, indicating significant hydrogenation and deconstruction (Fig. 9d). Conversely, the flexible W-Boat produces black tar-like oils, while the Foam product generates an auburn, brittle solid (Fig. 9d) and considerable yields of alkylaromatics (9%) and oligomers (33%). The low AAR for the W-Boat oils and Foam solids after reaction reveals limited hydrogenation, with the Foam solid's AAR

matching that of neat PS (Fig. 9b and Fig. S19). The deactivation of Ni/SiO_2 is associated with the performance additives in these PS products (Fig. 4). X-ray fluorescence (XRF) of the W-Boat identified a significant quantity (~5 wt%) of calcium likely as fine calcium carbonate ($CaCO_3$) nano/microparticles that are commonly added to plastics as a filler and mechanical property modifiers (i.e., improve PS flexibility)[61]. The surface of $CaCO_3$ particles is also often functionalized with organic and inorganic components to improve dispersion within the polymer via colloidal interactions and further tune mechanical properties[61]. Vacuum filtration, centrifugation, decanting, and other separation methods could not isolate the colloidally suspended $CaCO_3$ particles from the PS polymer. We suspect the $CaCO_3$ particles or the surface's functionalized components are responsible for the Ni/SiO_2 deactivation. Alternatively, expanded/extruded foams contain blowing agents, dispersion agents, foam stabilizers, and other additives to generate the porous foam structure[62]. These components could be responsible for the Ni deactivation as they can contain halogen, hydrazine, sulfonyl, and other organic functionalities[62].

3. Conclusions

In this study, we demonstrate nickel supported on silica (Ni/SiO_2) for polystyrene (PS) hydrogenolysis to lubricant base oils under mild conditions (300 °C and 70 bar H_2) within 6 h. Unlike polyolefins, the yield to methane and other gaseous hydrocarbons is small. Process optimization revealed that the yields of gas, liquid (i.e., alkanes, aromatics, and dimer and trimer oligomers), and oils are unaffected by temperature and H_2 pressures (P_H). However, GPC and NMR analysis of the oils reveals a reduction in the molecular weight distribution and significant hydrogenation of the aromatic rings in PS, respectively, at higher temperatures and P_H.

Furthermore, we have defined the alkyl-to-aromatic ratio (AAR) from ^{1}H NMR characterization that consolidates the complex structural changes of PS into a single parameter to simplify the oil analysis. Time-dependent PS hydrogenolysis experiments at 30 and 70 bar H_2 further demonstrate the strong dependence on P_H, while revealing hydrogenolysis occurs sequentially, requiring significant aromatic ring hydrogenation prior to reduction of the molecular weight. Rate analysis for 1,2-diphenylethane (DPE) hydrogenolysis exposes aromatic ring hydrogenation is 1000x faster than C-C bond cleavage over Ni/SiO_2, rationalizing the PS hydrogenolysis reaction pathway. After 6 h reactions, the oils show Group IV lubricant properties comparable to commercial synthetic oils and better to base oils produced from polypropylene hydrogenolysis. Lastly, Ni/SiO_2 catalysts are amenable to managing other virgin feedstocks and rigid commercial PS products, whereas flexible PS and packing foam products cause deactivation associated with the presence of additives. These results demonstrate high-quality lubricant base oils from PS using Ni/SiO_2, expanding the product slate for PS deconstruction technologies while exposing the importance of earth-abundant metals in the transition toward a circular economy.

4. Methods

4.1. Catalyst Synthesis

Nickel nitrate hexahydrate (Aldrich, $Ni(NO_3)_2$•$6H_2O$, ≥ 99.999% trace metal basis) was used as received and silica-gel (Sigma-Aldrich, SiO_2, Davisil grade 646, 35-60 mesh) was calcined in static air at 650 °C for 3 h (2 °C/min ramp) prior to synthesis. 15wt% Ni/SiO_2 was prepared via wetness impregnation of a nickel nitrate hexahydrate solution, dried in air at 110 °C, and then calcined at 550 °C for 3 h (2 °C/min ramp). Ni/SiO_2 was crushed and sieved to 63-125 μm (120-230 mesh) for reactions with 1,2-diphenylethane (DPE).

4.2. Catalyst Characterization

Ni/SiO_2 was characterized previously[15] using X-ray diffraction, N_2 sorption, transmission electron microscopy, and N_2O titrations.

4.3. Polystyrene Hydrogenolysis Reactions and Analysis

All polystyrene samples from Aldrich were used directly without any preprocessing. Commercial polystyrene products were cut into ~1 cm^2 pieces prior to reaction. Information on the polymer feedstocks is summarized in Table 2. Other chemicals and consumables used for product extraction and characterization are n-dodecane ($C_{12}H_{26}$, Thermo Scientific, 99 %), methanol (CH_3OH, Fisher Chemical, HPLC grade, ≥99.9%), methylene chloride (CH_2Cl_2, Fisher Chemical, HPLC grade, ≥99.9%), tetrahydrofuran (C_4H_8O, Fisher Chemical, ≥99.9%, unstabilized), chloroform-d (CCl_3D, Thermo Scientific, >99.8 atom% D, 0.02-0.03 v/v% TMS), and Whatman filter paper (GE, 11 μm).

*Table 2: **Polymer feedstocks used in hydrogenolysis reactions**. *Gel-permeation chromatography of commercial PS products was not conducted due to additives that could potentially damage the instrument.*

Feedstock Classification	**Polymer**	**Vendor**	**Molecular Weight from Vendor (kDa)**	**Molecular Weight from GPC Analysis* (kDa)**	**Referencing in Text**
Virgin Granules	Polystyrene	Sigma	~35	~97	PS97
	Polystyrene	Sigma	~180	~5300	PS5300
	Polystyrene	Sigma	~280	~6000	PS6000
Commercial Polystyrene Products	Weigh boat	Fisherbrand	-	-	W-boat
	Petri dish	Fisherbrand	-	-	Petridish
	Falcon Tube	Corning Falcon	-	-	F-Tube
	Expanded polystyrene foam	ULINE	-	-	Foam

Hydrogenolysis reactions were conducted in a 50 mL Parr stainless steel batch reactor with a pressure gauge, thermocouple, and 25.4 x 8 mm PTFE magnetic stir bar. A band heater connected to a PID controller was used to heat the reactor and maintain the reactor temperature. The reactor and band heater were wrapped in fiberglass insulation to decrease ramping time and improve temperature stability.

Prior to reactions, the Ni/SiO_2 catalyst was reduced in 100 mL/min equimolar He/H_2 at 450 °C for 2 h (10 °C/min ramp). All catalytic reactions were conducted solvent-free. 100 mg of catalyst was added with 2.0 g of PS substrate to the Parr reactor and the contents were well-mixed using a stir bar. The Parr reactor was sealed, connected to a calibrated semi-batch H_2 line (Scheme 1), and purged six times with 15 bar H_2. The reactor was then pressurized to a cold reactor pressure (18-40 bar) and then heated to reaction temperature (260-300 °C). Stirring was turned on at 500 rpm when the reactor reached 240 °C. Reactions were run for specified intervals (0.5 – 9 h) after the reactor reached reaction temperature. Additional H_2 was delivered to the reactor via a semi-batch line when the reactor fell ~2 bar below the desired reaction pressure. The needle valve to the H_2 cylinder and ball valve would be opened to charge the dosing line to the regulator pressure. The needle valve to the H_2 cylinder would then be closed. The initial pressure of the dosing line was recorded, then H_2 would be dosed to the Parr reactor by opening the reactor's needle valve until the reactor's pressure reached the desired reaction pressure. The final pressure of the dosing line was recorded and the quantity of dosed H_2 was back-calculated (Fig. S20, Equation S1-4) using the pressure drop in the dosing line. Upon reaching the reaction time, the reactor was quickly quenched in an ice bath. Product collection was conducted when the reactor reached 2 °C. Gas samples were collected from the Parr reactor headspace by charging into a 1 L Tedlar gas sampling bag and analyzed with GC-FID (Agilent HP-Plot/Q+PT GC column). The reactor was opened and

washed with ~20 mL of methanol containing 20 mg of n-dodecane as an internal standard to collect light hydrocarbons and oligomer fragments. This methanol mixture was separated from the solids via filtration, and products were quantified using a GC-FID (Supelco Vocol and Agilent HP-5 columns) and identified using a GC-MS (Agilent DB-1 column). Calibration coefficients and retention times for light products were measured by injection of hydrocarbons (Hydrocarbon Standard, 98537, Absolute Standards) and aromatics multi-mix standards (Volatiles Mix #1, 94855, Absolute Standards) (Fig. S21, Table S7-8). Fig. S22 contains a representative chromatogram of methanol-soluble reaction products.

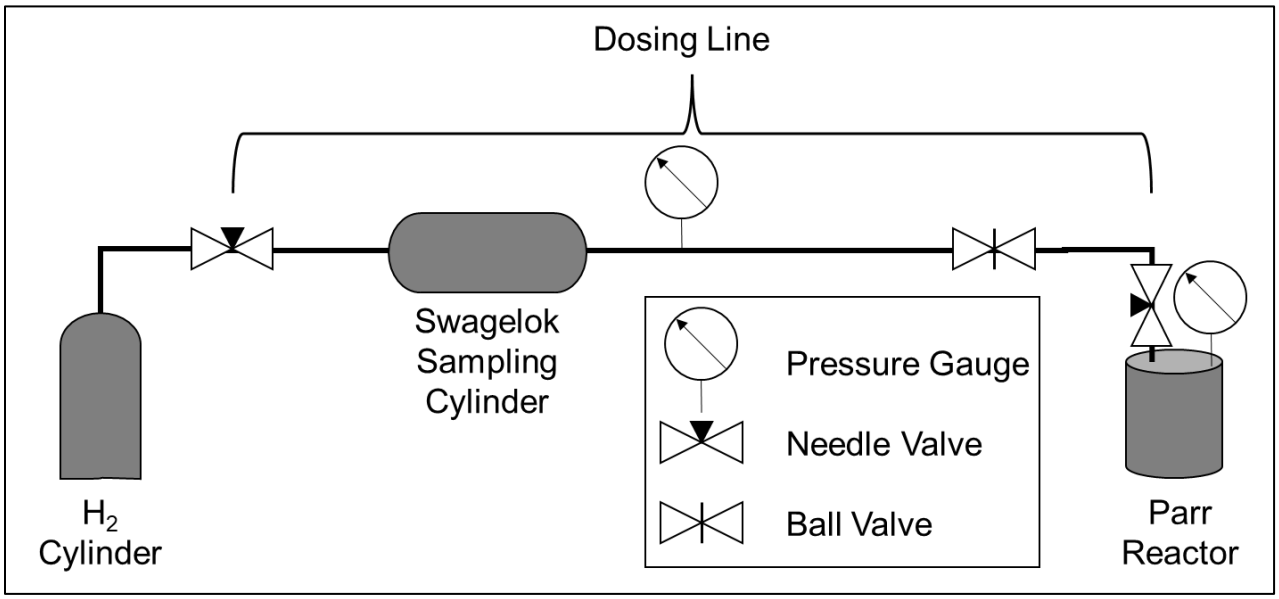

Scheme 1: Semi-batch H_2 dosing system schematic.

The remaining oils and unreacted PS were collected with ~20 mL of methylene chloride and filtered. Methylene chloride was removed using a rotary evaporator, and the oil mass was measured gravimetrically. A mass balance (MB) was conducted as follows:

$$MB = \frac{m_g + m_L + m_{oil}}{m_{PS,i}} \quad \text{Equation 1}$$

where m_g, m_L, m_{oil}, and $m_{PS,i}$ is the mass of gas, light hydrocarbons soluble in methanol, oils and unreacted PS dissolved in methylene chloride, and the initial mass of polystyrene, respectively. Product yields for group i was calculated as:

$$Y_i = \frac{m_i}{m_{PS,i}} \cdot 100\% \quad \text{Equation 2}$$

Oil products were analyzed using room temperature gel permeation chromatography (GPC) using Styragel HR 4, HR 3, and HR 0.5 columns (dimensions 4.6 × 300 mm) in tandem using THF as solvents (150 μL/min) and a Waters 2414 refractive index detector (RID). The retention times were calibrated using a Polystyrene Standards Kit (Waters, WAT058931, 0.500 kDa ≤ M_w 2500 Da). Yield distributions (y_o) were calculated as:

$$y_o = Y_o H_N(t) = Y_o \frac{H(t)}{\int H(t)dt} \quad \text{Equation 3}$$

where Y_o and $H_N(t)$ is the oil yield and normalized RID response, respectively. Deconvolution of yield distributions as a function of the logarithm of molecular weight were conducted using a custom MATLAB program. Briefly, the number of desired deconvoluted peaks and initial guesses for the peak's center(x_o), maximum intensity(I_{max}), and full-width at half-maximum $(FWHM)$ were input. An iterative least-squares method was employed to minimize the residuals between the fit's envelope and the yield distribution by adjustment of the three peak parameters. Additionally, the program could hold any or all of the peak parameters for a given peak when solving the peak deconvolution problem. Deconvoluted peaks were assumed to have Gaussian peak shapes, described by:

$$f_i(\log(M_w)) = I_{max} * \exp\left[-\frac{(log(M_w) - x_o)^2}{2\left(\frac{FWHM}{2\,ln(2)}\right)^2}\right] \quad \text{Equation 4}$$

GPC of the light oil fractions would occasionally become convoluted with the elution of the THF mobile phase. Deconvolution of the oil's yield distribution was adapted by adding a fourth peak to model the elution of the THF, while the lightest mode's peak center was fed an initial guess of the average peak position for this mode from other fittings ($x_o = 3.65$) and the range of values was constrained.

The chemical structure of the oil was analyzed using a liquid state NMR operating at a proton frequency of 400 MHz. NMR samples were prepared by adding ~40 mg of oil dissolved in 800 μL of d-chloroform. A standard ^{1}H quantitative NMR sequence was used with averaging over 16 scans. Integrations were done using the TopSpin software to calculate the alkyl-to-aromatic ratio (AAR) defined as:

$$AAR = \frac{A_{Alkyl}}{A_{Aro}} \quad \text{Equation 5}$$

where A_{Alkyl} is the integrated region from 0 to 2.5 ppm and A_{Aro} is the integrated region from 6 ppm to 8 ppm. The contribution of chloroform-d at 7.24 ppm was not included in the integration for the AAR calculation. A subsequent ^{13}C NMR experiment was run using a standard composite-pulse decoupling pulse sequence averaged over 1024 scans. This was used to calculate the PS conversion (X_{PS}) which is based on the presence of the methine carbon adjacent to an aromatic group in the PS carbon backbone which appears at 41 ppm[63]. Specifically, conversion is calculated as:

$$X_{PS} = \frac{A^{i}_{41ppm} - A^{f}_{41ppm}}{A^{i}_{41ppm}} \, x \, 100\% \qquad \text{Equation 6}$$

where A^{i}_{41ppm} is the normalized area of the methine carbon in the PS97 sample and A^{f}_{41ppm} is the normalized area of the methine carbon in the oil sample. All areas in Equation 6 are normalized to the sample's mass used in the NMR analysis.

The KV40 and KV100 of the product oils were measured using a Cannon 200 microviscometer. The viscometer was heated using a stirred mineral oil bath at the desired temperature (40 or 100 °C). For measurements, 200 µL of sample were added to the viscometer and vacuum was applied on the capillary side to raise the oil above the measurement zone. Care was taken to ensure bubbles were not present in the viscometer capillary. The vacuum was then removed to allow the oil to fall, and the time span for the sample to flow through the measurement zone was recorded in triplicate. Cannon N44 was used as a viscometer standard.

Pour points and oxidation onset temperatures were measured by Southwest Research Institute® according to ASTM D5949 and ASTM E2009 standardized protocol, respectively.

4.4. 1,2-Diphenylethane (DPE) Hydrogenolysis Reactions and Analysis

1-2-Diphenylethane ($C_{14}H_{14}$, TCI America, ≥99.0%) was used as received. Other chemicals and consumables used for product extraction and analysis are n-dodecane ($C_{12}H_{26}$, Thermo Scientific, 99 %), n-hexacosane ($C_{16}H_{34}$, Sigma, ≥%), methylene chloride (CH_2Cl_2, Fisher Chemical, HPLC grade, ≥99.9%), and Whatman filter paper (GE, 11 µm).

Ni/SiO_2 was crushed and sieved to 63-125 µm fraction for all reactions with 1-2-Diphenylethane (DPE). Batch hydrogenolysis reactions followed the same procedure as the polystyrene experiments, but 5-100 mg of sieved Ni/SiO_2 were added to the Parr reactor with 3 g

DPE and a PTFE stir bar. The reactor was connected to the semi-batch H_2 line, purged six times at 15 bar H_2, charged to 38 bar H_2, and began heating to 300 °C. Stirring was set to 500 rpm when the reactor hit 75 °C. Reactions were maintained for specified intervals (1 – 6 h) after reaching reaction temperature, with additional H_2 being delivered via the semi-batch line when the reactor pressure reached 48 bar. Reactions were stopped by quenching in an ice batch.

Gas samples were collected using a Tedlar gas bag when the reactor temperature reached 2 °C and analyzed with GC-FID (Agilent HP-Plot/Q+PT GC column). Liquid/solid reaction products were collected with ~20 mL of methylene chloride with 20 mg of dodecane. This solution was diluted 50-fold in methylene chloride, then quantified using a GC-FID (Agilent HP-1 column) and identified using a GC-MS (Agilent DB-1 column). Standards were prepared to measure the calibration coefficient for DPE.

For reactions in flow, DPE was dissolved to 10 wt% (with 1 wt% of n-hexadecane used as an internal standard) in n-dodecane (89 wt%). The reactor was a 150 mm long and 4.6 mm ID stainless steel HPLC tube (Restek) and placed vertically with flow going from bottom to top. The catalyst bed was held in place by quartz-wool, and inert rods were used to remove dead volume. The reactor was heated using a 1.5 in OD aluminum heat sink wrapped in heating tape (Omega, 210 W) connected to a PID controller. The temperature of the catalyst bed was measured directly using a thermocouple touching the bed's downstream side. Gas and liquid products were separated downstream of the back-pressure regulator using a custom-built separator submerged in an ice bath.

Prior to reaction, the reactor system was purged with He and pressurized with pure H_2 to reaction pressure (5-50 bar) with a back-pressure regulator (Equilibar, U3L series). The ex-situ

reduced and sieved Ni/SiO_2 was reduced in-situ with 20 mL/min of pure H_2 flow at 300 °C for 1 h to remove any passivated NiO. Upon reduction, the reaction temperature (150-300 °C) and gas flowrates (30-225 mL/min) were set. After stabilizing the reactor, the liquid feed was introduced at 200-1600 μL/min using an HPLC pump (Teledyne SSI, LS-class). Gas products were collected using a 1 L Tedlar gas bag, whereas liquid products were collected in GC vials. Liquid samples were diluted 50-fold in pure methylene chloride for GC analysis and gas samples were analyzed directly.

The DPE conversion (X_{DPE}) in batch reactions was defined as:

$$X_{DPE} = \frac{N_{DPE}^{i} - N_{DPE}^{f}}{N_{DPE}^{i}} \cdot 100\% \qquad \text{Equation 7}$$

where N_{DPE}^{i} and N_{DPE}^{f} are the total moles of DPE at the beginning and end of the reaction, respectively. The DPE residence time (τ) was defined as[64]:

$$\tau = t_{rxn} \cdot \frac{m_{cat}}{m_{DPE}} [=] min \qquad \text{Equation 8}$$

where t_{rxn} is the reaction time in minutes while m_{cat} and m_{DPE} are the catalyst and DPE masses, respectively. The DPE conversion in flow reactions was calculated as:

$$X_{DPE} = \sum_{j}^{n} \frac{\nu_j C_j}{C_{DPE}^{i}} \cdot 100\% \qquad \text{Equation 9}$$

where C_{DPE}^{i} is the molar concentrations of DPE in the reactor feed, C_j is the concentration of product j in the reactor effluent, and ν_j is the stoichiometric coefficient of product j. The reaction rate ($-r_{DPE}$) was approximated as:

$$-r_{DPE} = \frac{dC_{DPE}}{dt} \approx \frac{\Delta C_{DPE}}{\Delta t} = \frac{\dot{V}_o}{m_{cat}} \sum_j^n \nu_j C_j \ [=] \ \frac{mmol}{g_{cat} \cdot s} \qquad \text{Equation 10}$$

with $\dot{V}_o$ denoting the feed liquid volumetric flow rate to the reactor.

AUTHOR INFORMATION

Corresponding Author

Dionisios G. Vlachos – *Center for Plastics Innovation, University of Delaware, 221 Academy St., Newark, DE 19716, USA; Department of Chemical and Biomolecular Engineering, University of Delaware, 150 Academy St., Newark, DE 19716, USA.* Email: vlachos@udel.edu

Authors

Brandon C. Vance - *Center for Plastics Innovation, University of Delaware, 221 Academy St., Newark, DE 19716, USA; Department of Chemical and Biomolecular Engineering, University of Delaware, 150 Academy St., Newark, DE 19716, USA.*

Sean Najmi - *Center for Plastics Innovation, University of Delaware, 221 Academy St., Newark, DE 19716, USA.*

Author Contributions

B.C.V Conceptualization, Methodology, Investigation, Formal analysis, Writing - original draft, review & editing. **S.N.** Methodology, Investigation, Formal analysis, Writing - original draft, review & editing. **D.G.V.** Writing - review & editing, Project administration, Funding acquisition.

ASSOCIATED CONTENT

Supporting Information

The Supporting Information is available free of charge.

Polystyrene Hydrogenolysis to High-Quality Lubricants using Ni/SiO_2 SI

Data Availability

Data will be made available upon request.

Funding Sources

This work was supported as part of the Center for Plastics Innovation, an Energy Frontier Research Center funded by the U.S. Department of Energy, Office of Science, Basic Energy Sciences under Grant Number DE-SC0021166. B.C.V. acknowledges a Graduate Research Fellowship through the National Science Foundation under Grant Number 1940700. The authors used the NMR facilities at the University of Delaware, founded by the Delaware COBRE program, supported by a grant from the National Institute of General Medical Sciences - NIGMS (5 P30 GM110758–02) from the National Institutes of Health.

Notes

The authors declare no competing financial interest.

ABBREVIATIONS

PS, polystyrene; M_w, average molecular weight; Ni/SiO_2, nickel on silica; PVCH, polyvinyl-cyclohexane; P_H, hydrogen pressure; GCMS, gas chromatography mass spectrometry; GPC, gel-permeation chromatography; MWD, molecular weight distribution; NMR, nuclear magnetic resonance; AAR, alkyl-to-aromatic ratio; VI, viscosity index; DPE, 1,2-diphenylethane; CHBE, 1,2-cyclohexylbenzylethane; DCHE, 1,2-dicyclohexylethane; MCH, methylcyclohexane; TOL, toluene; nC26, n-hexacosane; XRF, X-ray fluorescence.

REFERENCES

(1) Rillig, M. C.; Kim, S. W.; Kim, T. Y.; Waldman, W. R. The Global Plastic Toxicity Debt. *Environ. Sci. Technol.* **2021**, *55* (5), 2717–2719. https://doi.org/10.1021/acs.est.0c07781.

(2) Sangkham, S.; Faikhaw, O.; Munkong, N.; Sakunkoo, P.; Arunlertaree, C.; Chavali, M.; Mousazadeh, M.; Tiwari, A. A Review on Microplastics and Nanoplastics in the Environment: Their Occurrence, Exposure Routes, Toxic Studies, and Potential Effects on Human Health. *Mar. Pollut. Bull.* **2022**, *181*, 113832. https://doi.org/10.1016/J.MARPOLBUL.2022.113832.

(3) Law, K. L.; Starr, N.; Siegler, T. R.; Jambeck, J. R.; Mallos, N. J.; Leonard, G. H. The United States' Contribution of Plastic Waste to Land and Ocean. *Sci. Adv.* **2020**, *6* (44), eabd0288. https://doi.org/10.1126/sciadv.abd0288.

(4) Lamb, J. B.; Willis, B. L.; Fiorenza, E. A.; Couch, C. S.; Howard, R.; Rader, D. N.; True, J. D.; Kelly, L. A.; Ahmad, A.; Jompa, J.; Harvell, C. D. Plastic Waste Associated with Disease on Coral Reefs. *Science (80-.).* **2018**, *359* (6374), 460–462. https://doi.org/10.1126/science.aar3320.

(5) OECD. *Global Plastics Outlook*; 2022. https://doi.org/10.1787/aa1edf33-en.

(6) EMF. *The New Plastics Economy: Rethinking the Future of Plastics & Catalysing Action*; 2017.

(7) Meys, R.; Bachmann, M.; Winter, B.; Zibunas, C.; Suh, S. Plastics By a Circular Carbon Economy. *Science (80-.).* **2021**, *76* (October), 71–76.

(8) Bachmann, M.; Zibunas, C.; Hartmann, J.; Tulus, V.; Suh, S.; Guillén-Gosálbez, G.; Bardow, A. Towards Circular Plastics within Planetary Boundaries. *Nat. Sustain.* **2023**, *6* (May). https://doi.org/10.1038/s41893-022-01054-9.

(9) Geyer, R.; Jambeck, J. R.; Law, K. L. Production, Use, and Fate of All Plastics Ever Made. *Sci. Adv.* **2017**, *3* (7), e1700782. https://doi.org/10.1126/sciadv.1700782.

(10) Lange, J. P. Managing Plastic Waste-Sorting, Recycling, Disposal, and Product Redesign. *ACS Sustain. Chem. Eng.* **2021**, *9* (47), 15722–15738.

https://doi.org/10.1021/ACSSUSCHEMENG.1C05013/ASSET/IMAGES/LARGE/SC1C05013_0001.JPEG.
(11) Schyns, Z. O. G.; Shaver, M. P. Mechanical Recycling of Packaging Plastics: A Review. *Macromol. Rapid Commun.* **2021**, *42* (3), 1–27. https://doi.org/10.1002/marc.202000415.
(12) Zhao, D.; Wang, X.; Miller, J. B.; Huber, G. W. The Chemistry and Kinetics of Polyethylene Pyrolysis: A Process to Produce Fuels and Chemicals. *ChemSusChem* **2020**, *13* (7), 1764–1774. https://doi.org/10.1002/cssc.201903434.
(13) Selvam, E.; Kots, P. A.; Hernandez, B.; Malhotra, A.; Chen, W.; Catala-Civera, J. M.; Santamaria, J.; Ierapetritou, M.; Vlachos, D. G. Plastic Waste Upgrade to Olefins via Mild Slurry Microwave Pyrolysis over Solid Acids. *Chem. Eng. J.* **2023**, *454*, 140332. https://doi.org/10.1016/J.CEJ.2022.140332.
(14) Briones, L.; Cordero, A.; Alonso-Doncel, M.; Serrano, D. P.; Escola, J. M. Catalytic Upgrading of a Model Polyethylene Pyrolysis Oil by Hydroconversion over Ni-Containing Hierarchical Beta Zeolites with Tailored Acidity. *Appl. Catal. B Environ.* **2024**, *341* (April 2023), 123359. https://doi.org/10.1016/j.apcatb.2023.123359.
(15) Vance, B. C.; Kots, P. A.; Wang, C.; Granite, J. E.; Vlachos, D. G. Ni/SiO2 Catalysts for Polyolefin Deconstruction via the Divergent Hydrogenolysis Mechanism. *Appl. Catal. B Environ.* **2023**, *322* (November 2022), 122138. https://doi.org/10.1016/j.apcatb.2022.122138.
(16) Vance, B. C.; Najmi, S.; Kots, P. A.; Wang, C.; Jeon, S.; Stach, E. A.; Zakharov, D. N.; Marinkovic, N.; Ehrlich, S. N.; Ma, L.; Vlachos, D. G. Structure-Property Relationships for Nickel Aluminate Catalysts in Polyethylene Hydrogenolysis with Low Methane Selectivity. *JACS Au* **2023**. https://doi.org/10.1021/jacsau.3c00232.
(17) Hinton, Z. R.; Kots, P. A.; Soukaseum, M.; Vance, B. C.; Vlachos, D. G.; Epps, T. H.; Korley, L. S. T. J. Antioxidant-Induced Transformations of a Metal-Acid Hydrocracking Catalyst in the Deconstruction of Polyethylene Waste. *Green Chem.* **2022**, *24* (19), 7332–7339. https://doi.org/10.1039/d2gc02503e.
(18) Borkar, S. S.; Helmer, R.; Panicker, S.; Shetty, M. Investigation into the Reaction Pathways and Catalyst Deactivation for Polyethylene Hydrogenolysis over Silica-Supported Cobalt Catalysts. *ACS Sustain. Chem. Eng.* **2023**. https://doi.org/10.1021/acssuschemeng.3c02202.
(19) Chen, L.; Meyer, L. C.; Kovarik, L.; Meira, D.; Pereira-Hernandez, X. I.; Shi, H.; Khivantsev, K.; Gutiérrez, O. Y.; Szanyi, J. Disordered, Sub-Nanometer Ru Structures on CeO 2 Are Highly Efficient and Selective Catalysts in Polymer Upcycling by Hydrogenolysis. *ACS Catal.* **2022**, *12* (8), 4618–4627. https://doi.org/10.1021/acscatal.2c00684.
(20) Tennakoon, A.; Wu, X.; Meirow, M.; Howell, D.; Willmon, J.; Yu, J.; Lamb, J. V.; Delferro, M.; Luijten, E.; Huang, W.; Sadow, A. D. Two Mesoporous Domains Are Better Than One for Catalytic Deconstruction of Polyolefins. *J. Am. Chem. Soc.* **2023**, *145* (32), 17936–17944. https://doi.org/10.1021/jacs.3c05447.
(21) Hackler, R. A.; Lamb, J. V.; Peczak, I. L.; Kennedy, R. M.; Kanbur, U.; Lapointe, A. M.; Poeppelmeier, K. R.; Sadow, A. D.; Delferro, M. Effect of Macro- and Microstructures on Catalytic Hydrogenolysis of Polyolefins. *Macromolecules* **2022**, *55* (15), 6801–6810. https://doi.org/10.1021/ACS.MACROMOL.2C00805/ASSET/IMAGES/LARGE/MA2C00805_0008.JPEG.
(22) Kots, P. A.; Liu, S.; Vance, B. C.; Wang, C.; Sheehan, J. D.; Vlachos, D. G. Polypropylene Plastic Waste Conversion to Lubricants over Ru/TiO2Catalysts. *ACS Catal.* **2021**, *11*,

8104–8115. https://doi.org/10.1021/acscatal.1c00874.
(23) Vance, B. C.; Kots, P. A.; Wang, C.; Hinton, Z. R.; Quinn, C. M.; Epps, T. H.; Korley, L. S. T. J.; Vlachos, D. G. Single Pot Catalyst Strategy to Branched Products via Adhesive Isomerization and Hydrocracking of Polyethylene over Platinum Tungstated Zirconia. *Appl. Catal. B Environ.* **2021**, *299*, 120483. https://doi.org/10.1016/j.apcatb.2021.120483.
(24) Li, L.; Luo, H.; Shao, Z.; Zhou, H.; Lu, J.; Chen, J.; Huang, C.; Zhang, S.; Liu, X.; Xia, L.; Li, J.; Wang, H.; Sun, Y. Converting Plastic Wastes to Naphtha for Closing the Plastic Loop. *J. Am. Chem. Soc.* **2023**, *145* (3), 1847–1854. https://doi.org/10.1021/jacs.2c11407.
(25) Qiu, Z.; Lin, S.; Chen, Z.; Chen, A.; Zhou, Y.; Cao, X.; Wang, Y.; Lin, B. L. A Reusable, Impurity-Tolerant and Noble Metal-Free Catalyst for Hydrocracking of Waste Polyolefins. *Sci. Adv.* **2023**, *9* (25), eadg5332. https://doi.org/10.1126/sciadv.adg5332.
(26) Liu, Y.; Qian, J.; Wang, J. Pyrolysis of Polystyrene Waste in a Fluidized-Bed Reactor to Obtain Styrene Monomer and Gasoline Fraction. *Fuel Process. Technol.* **2000**, *63* (1), 45–55. https://doi.org/10.1016/S0378-3820(99)00066-1.
(27) Karaduman, A.; Şimşek, E. H.; Çiçek, B.; Bilgesü, A. Y. Flash Pyrolysis of Polystyrene Wastes in a Free-Fall Reactor under Vacuum. *J. Anal. Appl. Pyrolysis* **2001**, *60* (2), 179–186. https://doi.org/10.1016/S0165-2370(00)00169-8.
(28) Marczewski, M.; Kamińska, E.; Marczewska, H.; Godek, M.; Rokicki, G.; Sokołowski, J. Catalytic Decomposition of Polystyrene. The Role of Acid and Basic Active Centers. *Appl. Catal. B Environ.* **2013**, *129*, 236–246. https://doi.org/10.1016/j.apcatb.2012.09.027.
(29) Artetxe, M.; Lopez, G.; Amutio, M.; Barbarias, I.; Arregi, A.; Aguado, R.; Bilbao, J.; Olazar, M. Styrene Recovery from Polystyrene by Flash Pyrolysis in a Conical Spouted Bed Reactor. *Waste Manag.* **2015**, *45*, 126–133. https://doi.org/10.1016/J.WASMAN.2015.05.034.
(30) Kumar, V.; Khan, A.; Rabnawaz, M. Efficient Depolymerization of Polystyrene with Table Salt and Oxidized Copper. *ACS Sustain. Chem. Eng.* **2021**. https://doi.org/10.1021/ACSSUSCHEMENG.1C08400/ASSET/IMAGES/LARGE/SC1C08400_0008.JPEG.
(31) Joshi, B.; Raghav, H.; Agrawal, A.; Vempatapu, B. P.; Ray, A.; Sarkar, B. Sustainable Production of Styrene from Catalytic Recycling of Polystyrene over Potassium Promoted Fe-Al2O3 Catalyst. *Sustain. Energy Fuels* **2023**, *7* (5), 1256–1264. https://doi.org/10.1039/d2se01584f.
(32) Zayoud, A.; Dao Thi, H.; Kusenberg, M.; Eschenbacher, A.; Kresovic, U.; Alderweireldt, N.; Djokic, M.; Van Geem, K. M. Pyrolysis of End-of-Life Polystyrene in a Pilot-Scale Reactor: Maximizing Styrene Production. *Waste Manag.* **2022**, *139* (September 2021), 85–95. https://doi.org/10.1016/j.wasman.2021.12.018.
(33) Kruse, T. M.; Woo, O. S.; Wong, H. W.; Khan, S. S.; Broadbelt, L. J. Mechanistic Modeling of Polymer Degradation: A Comprehensive Study of Polystyrene. *Macromolecules* **2002**, *35* (20), 7830–7844. https://doi.org/10.1021/ma020490a.
(34) Kruse, T. M.; Wong, H. W.; Broadbelt, L. J. Modeling the Evolution of the Full Polystyrene Molecular Weight Distribution during Polystyrene Pyrolysis. *Ind. Eng. Chem. Res.* **2003**, *42* (12), 2722–2735. https://doi.org/10.1021/IE020657O.
(35) Cao, R.; Zhang, M.-Q.; Hu, C.; Xiao, D.; Wang, M.; Ma, D. Catalytic Oxidation of Polystyrene to Aromatic Oxygenates over a Graphitic Carbon Nitride Catalyst. *Nat. Commun.* **2022**, *13* (1), 1–10. https://doi.org/10.1038/s41467-022-32510-x.
(36) Oh, S.; Stache, E. E. Chemical Upcycling of Commercial Polystyrene via Catalyst-

Controlled Photooxidation. *J. Am. Chem. Soc.* **2022**, *144* (13), 5745–5749. https://doi.org/10.1021/JACS.2C01411/SUPPL_FILE/JA2C01411_SI_001.PDF.
(37) Huang, Z.; Shanmugam, M.; Liu, Z.; Brookfield, A.; Bennett, E. L.; Guan, R.; Herrera, D. E. V.; Lopez-Sanchez, J. A.; Slater, A. G.; McInnes, E. J. L.; Qi, X.; Xiao, J. Chemical Recycling of Polystyrene to Valuable Chemicals via Selective Acid-Catalyzed Aerobic Oxidation under Visible Light. *J. Am. Chem. Soc.* **2022**, *144* (14), 6532–6542. https://doi.org/10.1021/JACS.2C01410.
(38) Peng, Z.; Chen, R.; Li, H. Heterogeneous Photocatalytic Oxidative Cleavage of Polystyrene to Aromatics at Room Temperature. *ACS Sustain. Chem. Eng.* **2023**. https://doi.org/10.1021/acssuschemeng.3c01282.
(39) Oh, S.; Stache, E. E. Mechanistic Insights Enable Divergent Product Selectivity in Catalyst-Controlled Photooxidative Degradation of Polystyrene. *ACS Catal.* **2023**, *13* (16), 10968–10975. https://doi.org/10.1021/acscatal.3c02516.
(40) Luo, X.; Zhan, J.; Mei, Q.; Zhang, S. Selective Oxidative Upgrade of Waste Polystyrene Plastics by Nitric Acid to Produce Benzoic Acid. *Green Chem.* **2023**, *25* (17), 6717–6727. https://doi.org/10.1039/d3gc00865g.
(41) Ong, A.; Teo, J. Y. Q.; Feng, Z.; Tan, T. T. Y.; Lim, J. Y. C. Organocatalytic Aerobic Oxidative Degradation of Polystyrene to Aromatic Acids. *ACS Sustain. Chem. Eng.* **2023**. https://doi.org/10.1021/acssuschemeng.3c01387.
(42) Rabot, C.; Chen, Y.; Lin, S. Y.; Miller, B.; Chiang, Y. M.; Oakley, C. E.; Oakley, B. R.; Wang, C. C. C.; Williams, T. J. Polystyrene Upcycling into Fungal Natural Products and a Biocontrol Agent. *J. Am. Chem. Soc.* **2023**, *145* (9), 5222–5230. https://doi.org/10.1021/jacs.2c12285.
(43) Sullivan, K. P.; Werner, A. Z.; Ramirez, K. J.; Ellis, L. D.; Bussard, J. R.; Black, B. A.; Brandner, D. G.; Bratti, F.; Buss, B. L.; Dong, X.; Haugen, S. J.; Ingraham, M. A.; Konev, M. O.; Michener, W. E.; Miscall, J.; Pardo, I.; Woodworth, S. P.; Guss, A. M.; Román-Leshkov, Y.; Stahl, S. S.; Beckham, G. T. Mixed Plastics Waste Valorization through Tandem Chemical Oxidation and Biological Funneling. *Science (80-.).* **2022**, *378* (6616), 207–211. https://doi.org/10.1126/science.abo4626.
(44) Staudinger, H.; Geiger, E.; Huber, E. Über Hochpolymere Verbindungen, 15. Mitteilung: Über Die Reduktion Des Polystyrols. *Berichte der Dtsch. Chem. Gesellschaft (A B Ser.* **1929**, *62* (1), 263–267. https://doi.org/10.1002/cber.19290620134.
(45) Staudinger, H.; Wiedersheim, V. Über Hochpolymere Verbindungen, 21. Mitteil.: Über Die Reduktion Des Poly-Styrols. *Berichte der Dtsch. Chem. Gesellschaft (A B Ser.* **1929**, *62* (8), 2406–2411. https://doi.org/https://doi.org/10.1002/cber.19290620880.
(46) Elias, H. G.; Etter, O. Glass Temperature of Hydrogenated Polystyrene. *J. Macromol. Sci. Part A - Chem.* **1967**, *1* (5), 943–953. https://doi.org/10.1080/10601326708053746.
(47) McGrath, M. P.; Sall, E. D.; Tremont, S. J. Functionalization of Polymers by Metal-Mediated Processes. *Chem. Rev.* **1995**, *95*, 381–398. https://doi.org/https://doi.org/10.1021/cr00034a004.
(48) Tennakoon, A.; Wu, X.; Paterson, A. L.; Patnaik, S.; Pei, Y.; LaPointe, A. M.; Ammal, S. C.; Hackler, R. A.; Heyden, A.; Slowing, I. I.; Coates, G. W.; Delferro, M.; Peters, B.; Huang, W.; Sadow, A. D.; Perras, F. A. Catalytic Upcycling of High-Density Polyethylene via a Processive Mechanism. *Nat. Catal.* **2020**, *3* (11), 893–901. https://doi.org/10.1038/s41929-020-00519-4.
(49) Meirow, M.; Tennakoon, A.; Wu, X.; Willmon, J.; Howell, D.; Huang, W.; Sadow, A. D.;

Luijten, E. Influence of Pore Length on Hydrogenolysis of Polyethylene within a Mesoporous Support Architecture. *J. Phys. Chem. C* **2023**. https://doi.org/10.1021/acs.jpcc.3c04300.
(50) Liu, S.; Josephson, T. R.; Athaley, A.; Chen, Q. P.; Norton, A.; Ierapetritou, M.; Siepmann, J. I.; Saha, B.; Vlachos, D. G. Renewable Lubricants with Tailored Molecular Architecture. *Sci. Adv.* **2019**, *5* (2). https://doi.org/10.1126/sciadv.aav5487.
(51) Verdier, S.; Coutinho, J. A. P.; Silva, A. M. S.; Alkilde, O. F.; Hansen, J. A. A Critical Approach to Viscosity Index. *Fuel* **2009**, *88* (11), 2199–2206. https://doi.org/10.1016/j.fuel.2009.05.016.
(52) Flaherty, D. W.; Uzun, A.; Iglesia, E. Catalytic Ring Opening of Cycloalkanes on Ir Clusters: Alkyl Substitution Effects on the Structure and Stability of C–C Bond Cleavage Transition States. *J. Phys. Chem. C* **2015**, *119* (5), 2597–2613. https://doi.org/10.1021/JP511688X.
(53) Leclercq, G.; Pietrzyk, S.; Peyrovi, M.; Karroua, M. Hydrogenolysis of Saturated Hydrocarbons. V. Influence of Hydrocarbon Structures on the Activity and Selectivity of Ni on Silica. *J. Catal.* **1986**, *99* (1), 1–11. https://doi.org/10.1016/0021-9517(86)90192-2.
(54) Matsumoto, H.; Saito, Y.; Yoneda, Y. The Classification of Metal Catalysts in Hydrogenolysis of Hexane Isomers. *J. Catal.* **1971**, *22* (2), 182–192. https://doi.org/10.1016/0021-9517(71)90184-9.
(55) Török, B.; Bartók, M. Hydrogenative Transformations of Methylcyclobutane over Silica-Supported Rh, Ni, Pt and Pd Catalysts at Different Temperatures. *Catal. Letters* **1994**, *27* (3–4), 281–287. https://doi.org/10.1007/BF00813914.
(56) Kochloefl, K.; Bažant, V. Hydrogenolysis of Saturated Hydrocarbons on a Nickel Catalyst. I. Kinetics of Hydrogenolysis of Ethylcyclohexane and Reactivity of Alkylcyclohexanes. *J. Catal.* **1967**, *8* (3), 250–260. https://doi.org/10.1016/0021-9517(67)90312-0.
(57) Robinson, P. R.; Dolbear, G. E. *Hydrotreating and Hydrocracking: Fundamentals BT - Practical Advances in Petroleum Processing*; 2006; Vol. 1.
(58) Mittendorfer, F.; Hafner, J. Hydrogenation of Benzene on Ni(111)A DFT Study. *J. Phys. Chem. B* **2002**, *106* (51), 13299–13305. https://doi.org/10.1021/JP026010Z.
(59) Bertolini, J. C.; Dalmai-Imelik, G.; Rousseau, J. Benzene Adsorption on Nickel (100) and (111) Faces Studied by Leed and High Resolution Electron Energy Loss Spectroscopy. *Surf. Sci.* **1977**, *67* (2), 478–479. https://doi.org/10.1016/0039-6028(77)90009-7.
(60) Ge, J.; Peters, B. Mass Transfer in Catalytic Depolymerization: External Effectiveness Factors and Serendipitous Processivity in Stagnant and Stirred Melts. *Chem. Eng. J.* **2023**, *466* (January), 143251. https://doi.org/10.1016/j.cej.2023.143251.
(61) Niu, Y. Q.; Liu, J. H.; Aymonier, C.; Fermani, S.; Kralj, D.; Falini, G.; Zhou, C. H. Calcium Carbonate: Controlled Synthesis, Surface Functionalization, and Nanostructured Materials. *Chem. Soc. Rev.* **2022**, *51* (18), 7883–7943. https://doi.org/10.1039/d1cs00519g.
(62) Wypych, G. *Handbook of Foaming and Blowing Agents*, 1st ed.; ChemTec Publishing: Toronto, 2017.
(63) Cheng, H. N.; Lee, G. H. NMR Studies of Polystyrene Tacticity. *Int. J. Polym. Anal. Charact.* **1996**, *2* (4), 439–455. https://doi.org/10.1080/10236669608033361.
(64) Jensen, C. U.; Guerrero, J. K. R.; Karatzos, S.; Olofsson, G.; Iversen, S. B. *Hydrofaction™ of Forestry Residues to Drop-in Renewable Transportation Fuels*; Elsevier Ltd., 2017. https://doi.org/10.1016/B978-0-08-101029-7.00009-6.

SYNOPSIS

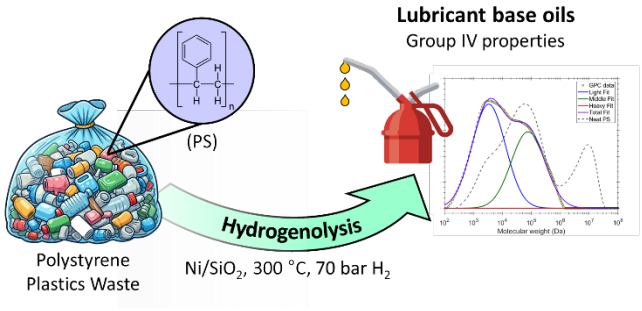
Lubricant base oils
Group IV properties
(PS)
Hydrogenolysis
Polystyrene
Plastics Waste
Ni/SiO2, 300 °C, 70 bar H2